ARTICLE OPEN

Check for updates

Dzyaloshinskii–Moriya interaction in noncentrosymmetric superlattices

Woo Seung Ham[1], Abdul-Muizz Pradipto [2,3✉], Kay Yakushiji [4], Kwangsu Kim[5], Sonny H. Rhim[5], Kohji Nakamura[2], Yoichi Shiota[1], Sanghoon Kim [5✉] and Teruo Ono [1✉]

Dzyaloshinskii–Moriya interaction (DMI) is considered as one of the most important energies for specific chiral textures such as magnetic skyrmions. The keys of generating DMI are the absence of structural inversion symmetry and exchange energy with spin–orbit coupling. Therefore, a vast majority of research activities about DMI are mainly limited to heavy metal/ferromagnet bilayer systems, only focusing on their interfaces. Here, we report an asymmetric band formation in a superlattices (SL) which arises from inversion symmetry breaking in stacking order of atomic layers, implying the role of bulk-like contribution. Such bulk DMI is more than 300% larger than simple sum of interfacial contribution. Moreover, the asymmetric band is largely affected by strong spin–orbit coupling, showing crucial role of a heavy metal even in the non-interfacial origin of DMI. Our work provides more degrees of freedom to design chiral magnets for spintronics applications.

INTRODUCTION

The lack of inversion symmetry at the interface between a heavy metal (HM) and a ferromagnet (FM) induces the antisymmetric exchange interaction so-called Dzyaloshinskii–Moriya interaction (DMI)[1–4]. Recently, DMI has been intensively studied in the material combinations possessing perpendicular magnetic aniso-tropy (PMA) due to their necessities in creating magnetic chiral textures, such as magnetic skyrmions for the new type of racetrack memory device[5–8]. Generally, in order to stabilize skyrmions at room temperature, multilayer structures with repetitive stacking of FM/HM bilayer are utilized because multi-stacking of the bilayer unit easily provide the PMA and the sizable DMI at the same time, both of them arising from the same physical origin, i.e., interfacial SOC[9–13]. In this respect, Co/Pd and Co/Pt interfaces are one of the well-known material combinations providing both the PMA and the DMI originating from interfaces, resulting in stable magnetic skyrmions[14,15]. With the same manner of such an AB-type multi-stacking structure composed of several nanometer-thick layers, a layer structure with ABC-type repetitive stacking of a few atomic monolayers is interesting system as illustrated in Fig. 1a. An epitome is the [Co/Pd/Pt] superlattice (SL) possessing PMA generated by the bulk-type spin momentum locking due to absence of inversion symmetry in stacking order[16]. Note that not interfaces but asymmetry of bulk-type band formation in the [Co/Pd/Pt]-SL as illustrated in Fig. 1b is essential to give rise to such a chiral phenomenon, resulting in strong PMA.

Such inversion symmetry breaking (ISB) in the SL with ABC-type stacking order would traditionally be accounted for by involving the Rashba model Hamiltonian, $\mathcal{H}_R = a_R(\mathbf{k} \times \hat{z}) \cdot \boldsymbol{\sigma}$, which was initially proposed for a surface, where $\hat{z}$ is the direction of inversion-symmetry-breaking-induced potential gradient[17]. The oddness of the SOC in the **k** space due to the ISB is shown by the dependence of the Hamiltonian on the linear terms in **k**, although higher odd-order may in principle also appear. Rashba effect manifests most immediately into a spin-splitting within the **k**

space, and it has been vastly utilized to interpret a number of magnetic phenomena[11,18–20], in particular those well understood to originate from the ISB, such as the DMI responsible for exotic magnetic textures such as skyrmions and chiral domain walls, and spin–orbit torque. It should be noted that amorphous ferrimagnet GdFeCo exhibits bulk DMI feature, which is independent of interface but due to inhomogeneous distribution of elemental content[21]. In this context, further study to distinguish DMI interface and bulk origin would be interesting topic.

In this study, we investigate DMI of the [Co/Pd/Pt]-SL arising from bulk spin-momentum locking. First-principles calculations reproduce such DMI enhancement in the SL, showing that the asymmetry of bands around Fermi energy level induced by ISB. The observed behavior of DMI upon increasing the repetitions of the ABC-layer unit in the SL suggests that while the interfacial and bulk DMI co-exist with small N, the enhancement of DMI with larger N can be attributed to the bulk-type asymmetric band formation around the Fermi level.

RESULTS AND DISCUSSION

DMI of the noncentrosymmetric SLs

Estimation of the magnetocrystalline energy (MCA) and DMI is done by following the steps outlined previously[22–24]. Here, we consider 1–4 [Co/Pt/Pd] units, and anticlockwise rotation of the spin-spiral structures as shown in Fig. 2a–c. The detailed process is explained in the "Method" section. The calculation results are summarized in Fig. 2d and e. The odd terms of the MCA energy (E_{MCA}^{odd}), which quantifies ISB, are summarized in Fig. 2d. This quantity is related to the ISB-induced shift of the band structure along the k_y direction due to the magnetization along x direction. We note that E_{MCA}^{odd} increases with the repetition number N of [Co/Pt/Pd] unit layers. The total MCA and E_{MCA}^{odd} in the [Pt/Co/Pd]$_N$ increases shown in Fig. 2d, and the total MCA value can be expected to reach 0.043 meV Å^{-2} obtained for the bulk [Co/Pt/Pd]-SL, i.e. the infinitely

[1]Institute for Chemical Research, Kyoto University, Uji, Kyoto, Japan. [2]Department of Physics Engineering, Mie University, Tsu, Mie, Japan. [3]Faculty of Mathematics and Natural Sciences, Institut Teknologi Bandung, Bandung, Indonesia. [4]National Institute of Advanced Industrial Science and Technology (AIST), Tsukuba, Ibaraki, Japan. [5]Department of Physics, University of Ulsan, Ulsan, South Korea. ✉email: a.m.t.pradipto@gmail.com; sanghoon.kim@ulsan.ac.kr; ono@scl.kyoto-u.ac.jp
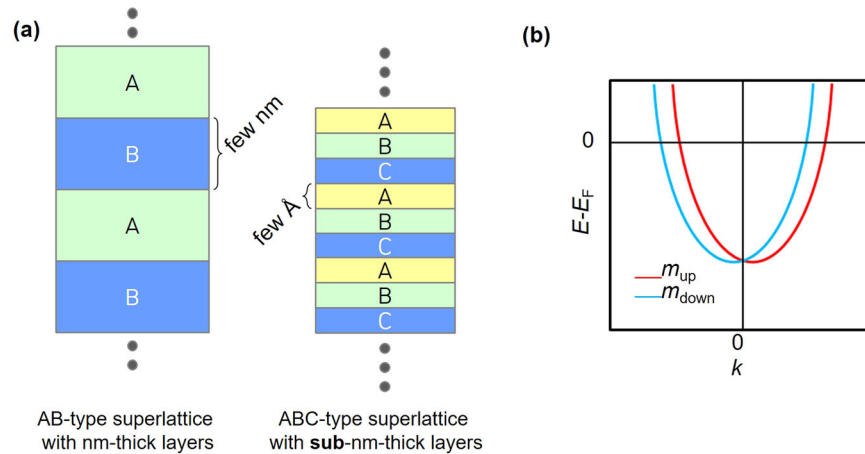
Fig. 1 SL structure with symmetry breaking in stacking order. a SLs with AB-type and ABC-type stacking-order, which is composed of nm-thick and sub-nm-thick layers, respectively. **b** Schematic image of an asymmetric band structure in terms of direction of magnetization in the SL with ABC-stacking order.

periodic system along c direction [Pt/Co/Pt]$_\infty$[16]. When the DMI constants are further extracted by utilizing the polynomial expression of the frozen magnon energy (Eq. 2 in "Method" section), we obtain a DMI energy density (**D**) value of the asymmetric [Pt/Co/Pd]$_N$ structure which increases with N [see Fig. 2e]. Here, we use the unit J m^{-2} for DMI values of the structures in order to compare with experimental results, shown later in this study. It is important to note that the **D** value increases with N and converges to the bulk value. Such linear dependence of DMI cannot be simply explained by the interfacial origin. If the increase in DMI with N is fully originated from the interfacial spin–orbit coupling, DMI should be independent of N because the gains in the DMI energy by increasing the number of interfaces are compensated by the volume of Co layers. The detailed mechanism of this result is explained in the following paragraph with anatomy of the **k**-dependent band structures.

The two-dimensional MCA contour map of [Pt/Co/Pd]$_1$ is shown in Fig. 3a. This map shows the typical characteristic of the MCA in the systems with ISB. Since the in-plane magnetization is oriented along the $+x$ direction, i.e., $\mathbf{m} = m_{+x}\hat{x}$, the MCA is asymmetric along the k_y axis, which is along the $\hat{z} \times \mathbf{m}$ direction, and shows mirror symmetry along k_x direction. Similar behavior is obtained for other N. The Fermi surface of [Pt/Co/Pd]$_1$ is visibly shifted towards negative k_y as shown by using the red color in Fig. 3b for m_{+x} magnetization, and is shifted symmetrically towards negative k_y when the magnetization is along the $m_{-x}\hat{x}$ direction, as plotted by using the blue color in Fig. 3b. In order to check the band contribution to the Rashba splitting, we plot Fermi surface by switching off the spin–orbit coupling in each atomic layer. Comparing the results shown in Fig. 3d–f, it is visible that switching off SOC in Pt layer alters the shape of the Fermi contour most considerably compared to that in Co and Pd. As the change in the Fermi contour indicates the modification of the band structure around the Fermi level, the result implies the crucial role of Pt bands to the band splitting, which should be attributed to the strong SOC constant of the Pt atom.

The anatomy of the DMI can be decomposed in a similar fashion. For this purpose, one can extract the DMI using the polynomial expression (Eq. 1 the in "Method" section) from the spiral structures built for several **q** vectors by switching on/off the SOC of a particular layer. In this work, however, we choose a simpler approach, i.e., by calculating the asymmetry between the energies of spiral structures with $\mathbf{q} = \pm 0.25$, of which the degeneracy is lifted due to the ISB. When the asymmetric energy in a total structure, which is correlated with DMI and defined here as the energy difference between $\mathbf{q} = \pm 0.25$ states, are denoted as

$E_{\mathbf{q}=\pm 0.25}^{\text{asym}}$, the contribution of a particular layer L to the asymmetric energy can be given as

$$E_{\mathbf{q}=\pm 0.25}^{\text{asym}}(L) = E_{\mathbf{q}=\pm 0.25}^{\text{asym}}(\text{tot}) - E_{\mathbf{q}=\pm 0.25}^{\text{asym}}(L_{\text{off}}) \tag{1}$$

where $E_{\mathbf{q}=\pm 0.25}^{\text{asym}}(\text{tot})$ is the asymmetric energy which includes the contribution of all layers, and $E_{\mathbf{q}=\pm 0.25}^{\text{asym}}(L_{\text{off}})$ is the asymmetric energy when the SOC contribution of layer L is switched off. The results are summarized in Fig. 4, clearly showing that, first of all, despite being the carrier of the magnetic moments, Co gives very small contribution to the DMI. In fact, the largest contribution to the asymmetric energy, hence to the DMI, is coming from the neighboring Pt layers, which can be understood to dominate the band around Fermi level, as shown in Fig. 3d–f. It should be noted that for all N, Pd gives smaller and opposite contribution to the DMI, in comparison to Pt. Additionally, the evaluated total $E_{\mathbf{q}\pm 0.25}^{\text{asym}}$ for all N, as plotted in the inset of Fig. 4, shows considerable deviations for all contributions, then, converges to that of the bulk with infinite periodicity. This implies the existence of a non-interfacial origin, but bulk spin-momentum locking[25] for the DMI in the considered [Pt/Co/Pd]-SL systems.

Experimental observation of DMI of the noncentrosymmetric SLs

To experimentally confirm the bulk spin-momentum locking for the DMI, the [Co 0.4/Pd 0.4/Pt 0.4 (nm)] SLs, hereafter [Co/Pd/Pt]-SL, was prepared as the noncentrosymmetric SL varying N as explained in the "Method" section [see also Fig. 5a]. The X-ray reflection pattern of the film with $N = 5$ clearly shows the 1st-Bragg-like peak, implying that the [Co/Pd/Pt] unit structure is well preserved without severe atomic intermixing in spite of such ultra-thin thickness range[26,27]. All [Co/Pd/Pt]-SLs are confirmed to have PMA as shown in Fig. 5c and d. In Particular, all magnetic hysteresis curves measured with the easy-axis field sweep show squareness of unity and sharp switching properties of the SLs. In case of the hard-axis loops taken with in-plane field sweep, any signal jump in the loops was not observed, showing saturation at higher than 1 T. When $N > 2$, the saturation field becomes about 2 T. Thus, the films have strong PMA property with good coherency even though they have complexed layer structures.

In order to estimate the DMI energy of each SL, the measurement based on the extended droplet model was conducted[28,29]. Figure 6a shows the schematic illustration of the droplet measurement. Since the nucleated magnetic droplet possesses domain wall magnetizations with two opposite radial direction. As illustrated in Fig. 6a, we can consider two domain wall magnetizations ($\mathbf{M}_{\text{DW1}}$ and $\mathbf{M}_{\text{DW2}}$) with respect to H_x. If we
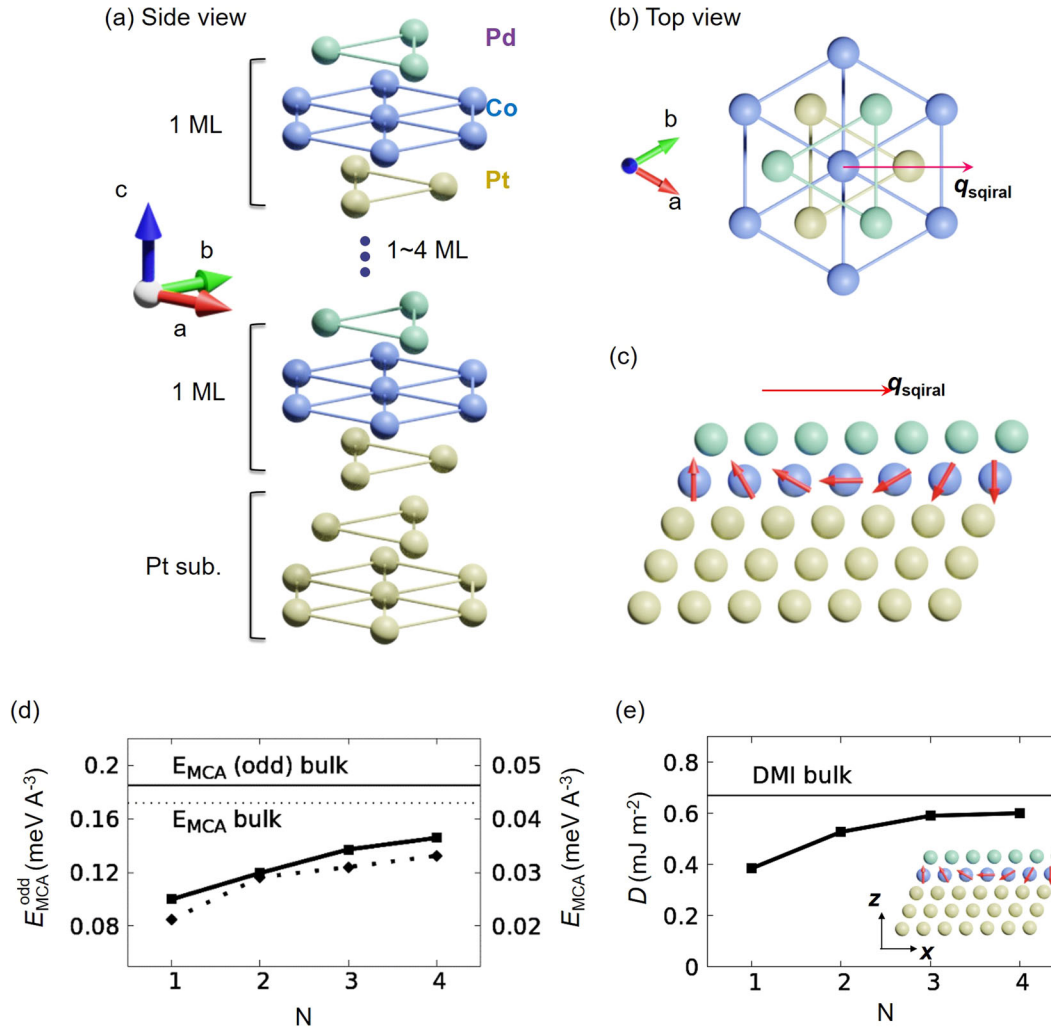
Fig. 2 ISB-related MCA energy and DMI of the [Co/Pt/Pd]-SL. a The side view and **b** the top view of the model crystal structure of Co/Pt/Pd-based multilayer system. The **M** direction for the propagation of the spin-spiral wave is indicated by the red arrow in (**b**). **c** Anticlockwise rotation of the spin-spiral structures. The calculated N dependence of **d** the odd term of MCA energies E_{MCA}^{odd} and **e** the DMI for the $[Pt/Co/Pd]_N$ model systems, while those obtained for the bulk system are shown using straight lines. The N dependence of the total MCA energies E_{MCA} of the $[Pt/Co/Pd]_N$ model systems and the corresponding bulk value are shown in (**d**) using dashed lines.

approximate that the two domain wall magnetizations dominate the total domain wall energy under H_x, the total domain wall energy of nucleated magnetic droplet can be obtained from sum of the domain wall energies: $\sigma_{total} = \sigma_{DW1}(+H_x) + \sigma_{DW2}(-H_x)$, where $\sigma_{DW1}(+H_x)$ and $\sigma_{DW1}(-H_x)$ are the domain wall energies with respect to H_x. The nucleation field through the relation is as follows: $\mu_0 H_n = \pi \sigma_{DW,total}^2 t_{FM}/2\mu_0 M_S p k_B T$, where t_{FM} is the ferromagnet thickness, $\mu_0 M_S$ is the saturation magnetization, p represents the thermal stability factor, k_B is the Boltzmann constant, and T denotes temperature[30]. Therefore, σ_{total} is proportional to $\sqrt{H_{n,z}}$ when $H_x > H_{DMI}$, otherwise σ_{total} becomes constant. The crossing point of the two linear curves can be defined as DMI-induced effective field (H_{DMI}). Based on this model, the angular dependence of coercivity was measured to obtain $\sqrt{H_{n,z}}$ of the SLs as illustrated in inset of Fig. 6 (b). In this measurement concept, applied magnetic field can be decomposed into H_x and $H_{n,z}$. The detailed measurement scheme is as follows; first of all, the sample is saturated to the $+z$ direction. Then, the magnetic field is swept from the positive to negative field in terms of various polar angles (θ) in order to obtain the θ dependence of switching field (H_{SW}). Considering the measurement time scale (ramping rate ~1 T/min.) is much slower than that

of complete switching via domain wall propagation initiated from the nucleation, we can consider the relation of $\mu_0 H_{n,z} = \mu_0 H_{SW} \cos\theta$. The angular dependence of the H_{SW} was obtained from the anomalous Hall effect measurement in terms of θ [see Fig. 6b]. Every SLs shows sharp switching behavior as shown in Fig. 6b. With this approach, we could obtain the quantitative information of DMI by plotting the H_x dependence of $\sqrt{H_{n,z}}$.

H_{DMI} values for all N values with each SL are clearly determined with the H_x vs. $\sqrt{H_{n,z}}$ plots as shown in Fig. 6c with arrows. The measured data show that H_{DMI} values of [Co/Pd/Pt]-SLs are N-dependent. Here, **D** should be discussed for precise discussion with excluding effects of K_{eff} and M_S, based on the relation $D = \mu_0 M_S \Delta H_{DMI}$, where Δ denotes the domain wall width which is determined by the exchange stiffness constant (A) and K_{eff} by $\Delta = \sqrt{A/K_{eff}}$. In all samples, $A = 10$ pJ m^{-1} is assumed since A in ultra-thin Co layers are usually an order of a few (typically 1–15) pJ m^{-1}[31,32].

Note that difference of DMI between Pt/Co and Co/Pd interfaces in the [Co/Pd/Pt]-SL can also enhance total DMI energy and the value should be larger than other symmetric structures. In other words, the interfacial origin should be also considered to explain our observation.
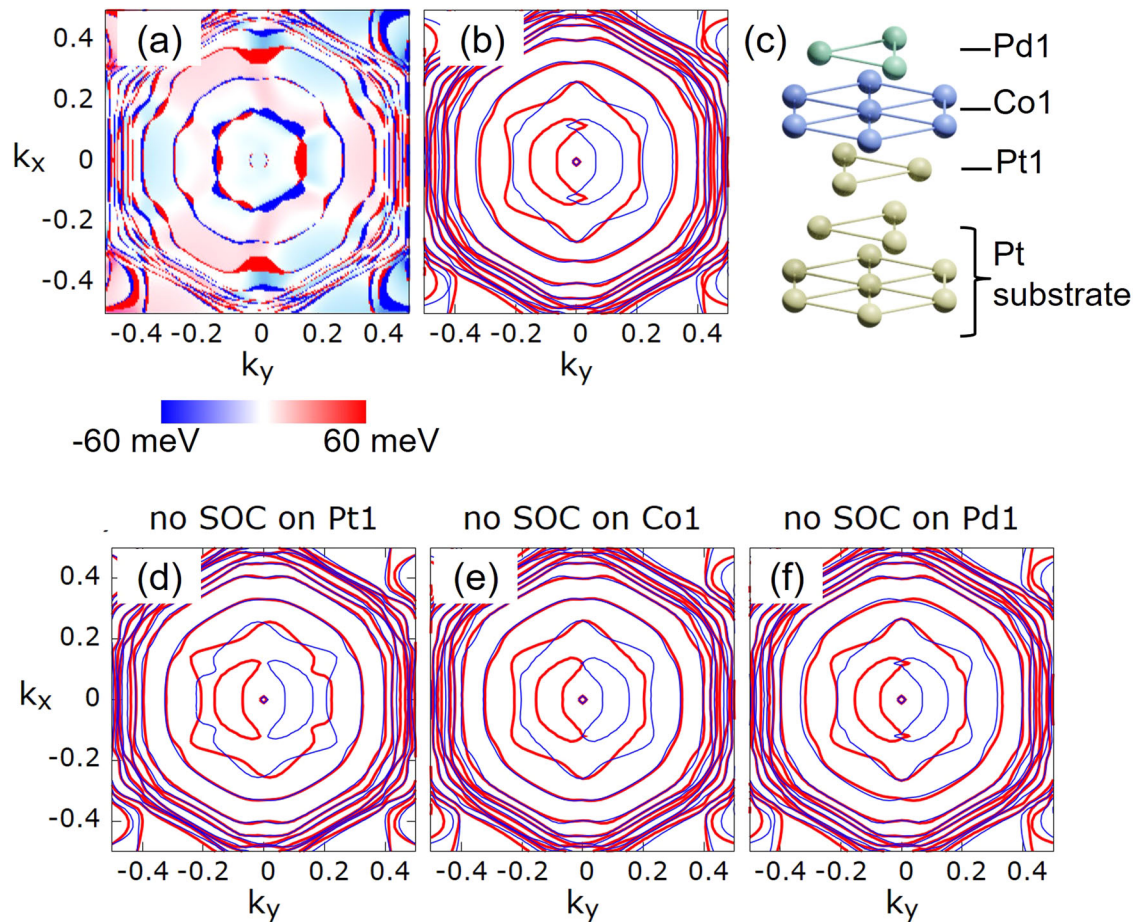
Fig. 3 k-dependent MCA energy and Fermi surface in the [Pt/Co/Pd] unit structure. a Two-dimensional (k_x, k_y) contour map of **k**-dependent MCA energy and **b** Fermi surface for different in-plane magnetization directions along +x and −x axes, plotted using respectively red and blue lines, of the [Pt/Co/Pd]$_1$ model system depicted in (**c**). **d**–**f** Fermi surface of the [Pt/Co/Pd]$_1$ model system in the absence of SOC on the Pt1, Co1, and Pd1 layer, respectively.

In order to confirm the characteristics of DMI originating from the interface, the dependence of repetition number (N) was studied in all series of the SLs. Figure 6d shows that the [Co/Pd/Pt]-SL shows N-dependence of DMI. Such increase of DMI in the [Pt/Co/Pd]$_N$ is fully consistent with our theoretical works. Especially, DMI of the [Co/Pd/Pt]-SL linearly increases by more than 300% when N increases from 2 to 10. Such behavior cannot be simply explained by the interfacial origin. We should note here that in order to reproduce the calculation results in our experiment, we used the smallest possible thickness of each layer which is about thickness of two atomic monolayers. Our XRR study in Fig. 4 proves well-defined layer structures. One atomic monolayer as shown in our DFT calculation is difficult to have continuous film in reality. Therefore, there should be both the conventional interface and Rashba-type bulk contributions simultaneously for our experimental observation, while the latter is dominant for the calculation especially with larger repetition numbers. Although quantitative comparison between calculation and experimental results is limited in this study, both results manifest that DMI in such an ABC-type structure cannot be explained with conventional approach with interfacial origin, indicating formation of asymmetric band structure. We also note that **D** has the linear relation with uniaxial magnetic anisotropy (K_u) estimated from the magnetic hysteresis loops shown in Fig. 5c and d as shown in Fig. 6e. Our results suggest that the enhancements of both **D** and PMA have the same origin in the Rashba SLs, namely the bulk spin-momentum locking[16].

Our experimental and theoretical studies demonstrate that the bulk spin-momentum locking in a SL can be made with asymmetric atomic stacking and structural coherency. Especially, the N-dependence of DMI of the [Co/Pd/Pt]-SL is an important phenomenon arising from the band asymmetry. So far, material selection has been limited to several cases for the development of skyrmion-based devices. On the other hand, bulk DMI can be made with such ABC-type material combination within atomic scale, which is larger than interfacial contribution. Hence, our experimental and theoretical findings can provide more options to design chiral magnet for spintronic devices. As a final remark, in two-dimensional system with C_{3v} symmetry, only non-Lifshitz invariant DMI can exist[33]. Our observation is related to this non-Lifshitz invariant but Lifshitz invariant terms dominate as the SL is three-dimensional object with strong two-dimensional feature inherent from interface. The noncentrosymmetric SL in this sense would invite further study on Lifshitz invariant contribution in DMI.

METHODS

Experiment

The [Co/Pd/Pt]-SL were deposited by the UHV magnetron sputtering system. The thickness of magnetic layer (Co) is varied in each SL. The static magnetic properties such as **M**$_s$ and magnetic anisotropy energy are investigated by the vibrating sample magnetometer (VSM). In order to quantify DMI energy, we used the extended droplet method[24–26]. All the films were patterned into a microstrip with a Hall bar structure by E-beam lithography to prevent the nucleation of domain at the rough microstrip
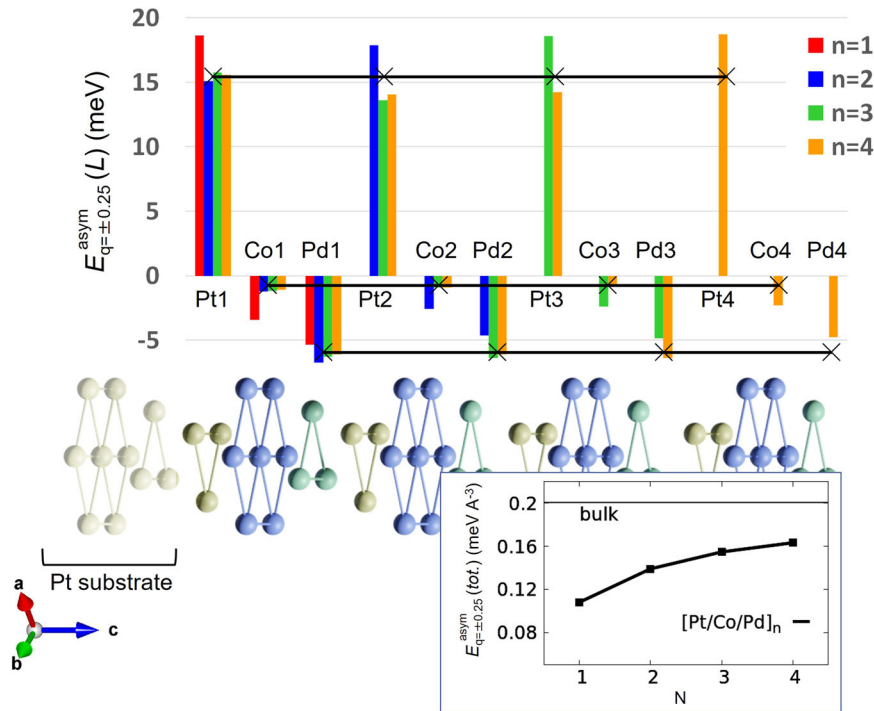
Fig. 4 Origin of the N-dependence of DMI in the [Pt/Co/Pd]-SL. The contribution of different atomic layer L to the asymmetric energy between the spiral structures with wave vectors $\mathbf{q} = \pm 0.25$, $E_{\mathbf{q}=\pm0.25}^{asym}(L)$. The corresponding atomic layer contributions for bulk system, i.e. with $N = \infty$, are shown with black lines. The sequence of the layers is illustrated. The total asymmetric energy $E_{\mathbf{q}=\pm0.25}^{asym}(tot)$ is also shown.
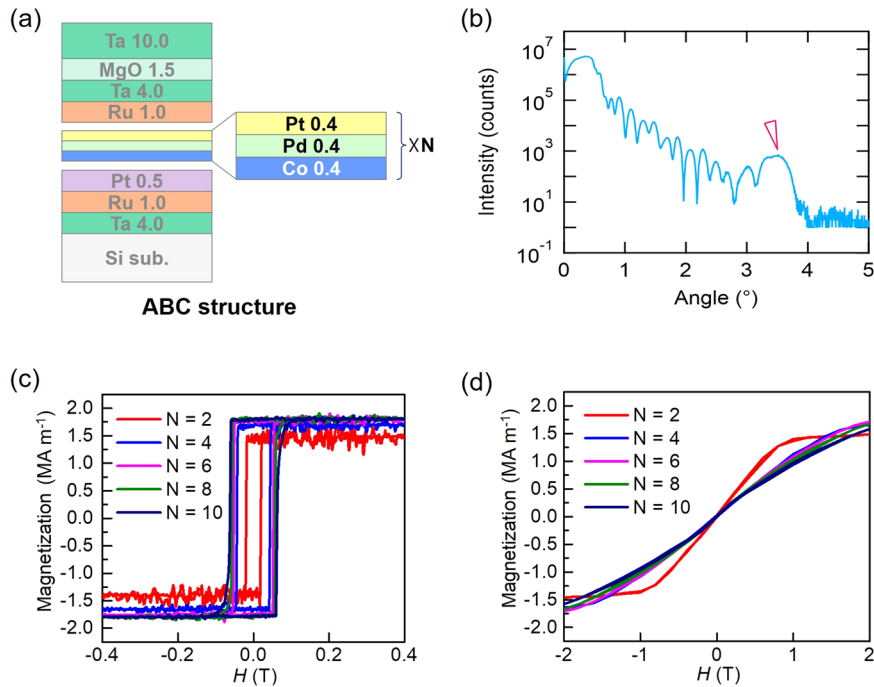

Fig. 5 Magnetic properties of the [Co/Pd/Pt] SLs. a A layer structure of the Co/Pd/Pt SLs. **b** XRR measurement result with the Co/Pd/Pt SL with $N = 5$. Magnetic hysteresis curves with **c** out-of-plane and **d** in-plane magnetic fields.

edge. Ti (5 nm)/Au (100 nm) electrodes are defined to make electrical contacts with μm-scale Hall bars by photolithography and lift-off process.

The first principles calculations for MCA and DMI of SLs

Our first-principles DFT calculations are based on the Generalized Gradient Approximation[34] as implemented in the Full-Potential Linearized

Augmented Plane Wave (FLAPW) code[21]. The MCA energy E_{MCA} has been defined in our calculation as the energy difference between the in- and out-of-plane magnetization direction, i.e., $E_{MCA} = E_{ip} - E_{op}$, where E_{ip} and E_{op} refer respectively to the total energy of the in- and out-of-plane magnetization. The inclusion of SOC is done via the second variational method[21]. The in-plane magnetization direction has been chosen to be along the x direction. We found that our calculated MCA energy has
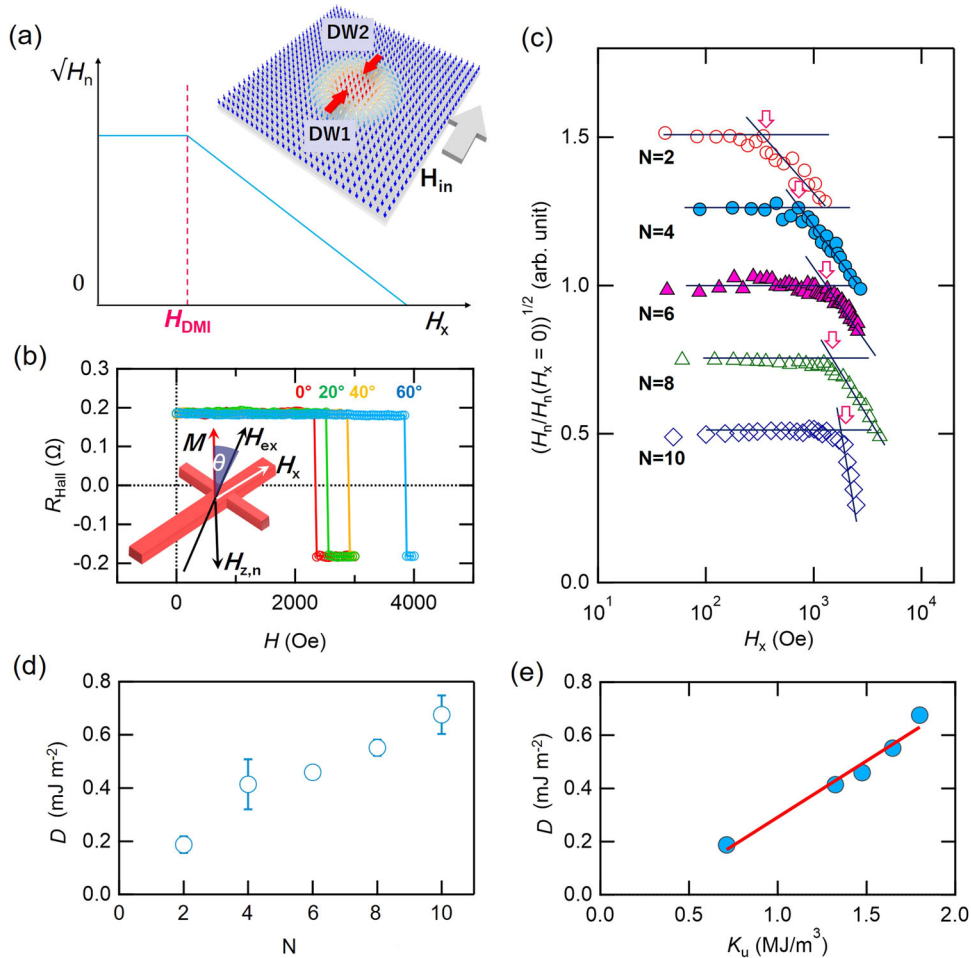
Fig. 6 N-dependent DMI of the [Co/Pd/Pt]-SL. a Illustration of droplet nucleation field profile in terms of in-plane field. **b** H_{SW} of the [Co/Pd/Pt]-SL with $N = 6$ measured using anomalous Hall effect in terms of θ. Inset shows the configuration of a device with external field (H_{ex}), components of the H_{ex} (H_x and H_z), and M_s. Solid lines are the fitting results before and after the threshold field. **c** Normalized $\sqrt{H_{n,z}}$ vs. H_x plots in terms of N. The solid lines indicate the fitted lines when $H_x < H_{DMI}$ and $H_x > H_{DMI}$. H_{DMI} values can be obtained from crossing points indicated by the arrows. **d** D values of the SLs in terms of N. **e** K_u vs. **D** plots. The red solid line is the linearly fitted line. The error bars represent standard deviations from the best fit.

converged at a relatively large two-dimensional **k**-point mesh of 100 × 100. In addition to the total MCA energy, we also virtually decomposed the **k**-dependent MCA energy into $E_{MCA}^{+k_y}$ and $E_{MCA}^{-k_y}$ in which $E_{MCA}^{\pm k_y} = E(m_x, \pm k_y) - E(m_z, \pm k_y)$ and calculated the odd term of the MCA energy E_{MCA}^{odd} by following the recipe in our previous work[16], as $E_{MCA}^{odd} = E_{MCA}^{+k_y} - E_{MCA}^{-k_y}$. This quantity, despite the fact that it contains no physical meaning, illustrates the physics of Rashba spin–orbit coupling and provides an estimation of the degree of ISB by the shift of the Fermi surface. Comparison with bulk values has been done with a three-dimensional k-point mesh of 75 × 75 × 45 for the bulk [Co/Pt/Pd]-SL[16].

The estimation of **D** values was done by following the steps outlined previously[23,24] We start from the ferromagnetic configuration which is found to be the ground state of all model systems at the scalar relativistic approximation, i.e., without the SOC. Next a set of spiral spin structures with wave vectors $\mathbf{q} = a/\lambda$ along the $M = (1, 1, 0)$ direction (see Fig. 3b), where λ is the wavelengths of the spin-spiral structures, are generated by utilizing the generalized Bloch theorem[35,36]. When the SOC is then included, the spin-spiral structures have been assumed to be the Néel xz out-of-plane rotation type. The frozen magnon energy, E(q), for **q** = 0, ±0.1, ±0.2, ±0.25 has been fitted with a polynomial expansion;

$$E(q) = C_0 + C_1\mathbf{q} + C_2\mathbf{q}^2 + C_3\mathbf{q}^3 + C_4\mathbf{q}^4 \qquad (2)$$

where the odd terms C_1 and C_3 occur due to the presence of ISB. The DMI discussed in this work is extracted as the antisymmetric exchange stiffness constant C_1, i.e., first order in **q**, or $\mathbf{D} \equiv C_1$. Convergence of the calculated DMI has been obtained with a 40 × 40 **k**−point mesh within

the two-dimensional Brillouin zone. As in the case of MCA energy, we have also computed the DMI for the bulk CoPtPd system with the Néel xz out-of-plane rotation type magnetic structures along the **M** direction, and a three-dimensional 40 × 40 × 20 **k**-point mesh has been used.

REFERENCES

1. Dzyaloshinskii, I. E. Thermodynamic theory of "Weak" ferromagnetism in anti-ferromagnetic substances. *Sov. Phys. JETP.* **5**, 1259 (1957).
2. Moriya, T. New mechanism of anisotropic superexchange interaction. *Phys. Rev. Lett.* **4**, 228–230 (1960).

3. Moriya, T. Anisotropic superexchange interaction and weak ferromagnetism. *Phys. Rev.* **120**, 91 (1960).

4. Heide, M., Bihlmayer, G. & Blügel, S. Dzyaloshinskii-Moriya interaction accounting for the orientation of magnetic domains in ultrathin films: Fe/W(110). *Phys. Rev. B* **78**, 140403 (2008).

5. Fert, A., Cros, V. & Sampaio, J. Skyrmions on the track. *Nat. Nanotechnol.* **8**, 152–156 (2013).

6. Emori, S., Bauer, U., Ahn, S.-M., Martinez, E. & Beach, G. S. D. Current-driven dynamics of chiral ferromagnetic domain walls. *Nat. Mater.* **12**, 611–616 (2013).

7. Boulle, O. et al. Room temperature chiral magnetic skyrmions in ultrathin magnetic nanostructures. *Nat. Nanotechnol.* **11**, 449–454 (2016).

8. Song, K. M. et al. Skyrmion-based artificial synapses for neuromorphic computing. *Nat. Electron.* **3**, 148–155 (2020).

9. Woo, S. et al. Observation of room-temperature magnetic skyrmions and their current-driven dynamics in ultrathin metallic ferromagnets. *Nat. Mater.* **15**, 501–506 (2016).

10. Jiang, W. et al. Skyrmions in magnetic multilayers. *Phys. Rep.* **704**, 1–49 (2017).

11. Yang, H. et al. Significant Dzyaloshinskii–Moriya interaction at graphene–ferromagnet interfaces due to the Rashba effect. *Nat. Mater.* **17**, 605 (2018).

12. Kundu, A. & Zhang, S. Dzyaloshinskii-Moriya interaction mediated by spin-polarized band with Rashba spin-orbit coupling. *Phys. Rev. B* **92**, 094434 (2015).

13. Di, K. et al. Direct observation of the Dzyaloshinskii-Moriya interaction in a Pt/Co/Ni film. *Phys. Rev. Lett.* **114**, 047201 (2015).

14. Pollard, S. D. et al. Observation of stable Neel skyrmions in cobalt/palladium multilayers with Lorentz transmission electron microscopy. *Nat. Commun.* **8**, 14761 (2017).

15. Gilbert, D. A. et al. Realization of ground-state artificial skyrmion lattices at room temperature. *Nat. Commun.* **6**, 8462 (2015).

16. Pradipto, A.-M. et al. Enhanced perpendicular magnetocrystalline anisotropy energy in an artificial magnetic material with bulk spin-momentum coupling. *Phys. Rev. B* **99**, 180410 (2019).

17. Bychkov, Y. A. & Rashba, E. I. Properties of a 2D electron gas with lifted spectral degeneracy. *JETP Lett.* **39**, 78 (1984).

18. Kim, K.-W. et al. Chirality from interfacial spin-orbit coupling effects in magnetic bilayers. *Phys. Rev. Lett.* **111**, 216601 (2013).

19. Barnes, S., Ieda, J. & Maekawa, S. Rashba spin-orbit anisotropy and the electric field control of magnetism. *Sci. Rep.* **4**, 4105 (2015).

20. Yang, H. et al. Anatomy and giant enhancement of the perpendicular magnetic anisotropy of cobalt–graphene heterostructures. *Nano Lett.* **16**, 145 (2016).

21. Kim, S. et al. Bulk Dzyaloshinskii–Moriya interaction in amorphous ferrimagnetic alloys. *Nat. Mater.* **18**, 685–690 (2019).

22. Nakamura, K. et al. Enhancement of magnetocrystalline anisotropy in ferromagnetic Fe films by intra-atomic noncollinear magnetism. *Phys. Rev. B* **67**, 014420 (2003).

23. Yamamoto, K. et al. Interfacial Dzyaloshinskii-Moriya interaction and orbital magnetic moments of metallic multilayer films. *AIP Adv.* **7**, 056302 (2017).

24. Nakamura, K. et al. Symmetric and asymmetric exchange stiffnesses of transition-metal thin film interfaces in external electric field. *J. Magn. Magn. Mater.* **457**, 97 (2018).

25. Bahramy, M. S. & Ogawa, N. Bulk Rashba semiconductors and related quantum phenomena. *Adv. Mater.* **29**, 1605911 (2017).

26. Yao, B. & Coiffey, K. R. The influence of periodicity on the structures and properties of annealed [Fe/Pt]n multilayer films. *J. Mag. Mag. Mater.* **320**, 559 (2008).

27. Yu, Y. S. et al. Structure and magnetic properties of magnetron-sputtered FePt/Au superlattice films. *J. Phys. D.; Appl. Phys.* **41**, 245003 (2008).

28. Kim, S. et al. Magnetic droplet nucleation with a homochiral Neel domain wall. *Phys. Rev. B.* **95**, 220402 (2017).

29. Kim, S. et al. Correlation of the Dzyaloshinskii-Moriya interaction with Heisenberg exchange and orbital asphericity. *Nat. Commun.* **9**, 1648 (2018).

30. Pizzini, S. et al. Chirality-Induced asymmetric magnetic nucleation in Pt/Co/AlOx ultrathin microstructures. *Phys. Rev. Lett.* **113**, 047203 (2014).

31. Eyrich, C. et al. Effects of substitution on the exchange stiffness and magnetization of Co films. *Phys. Rev. B* **90**, 235408 (2014).

32. Shim, J. H. et al. Ultrafast dynamics of exchange stiffness in Co/Pt multilayer. *Commun. Phys.* **2**, 74 (2020).

33. Ado, I. A. et al. Chiral ferromagnetism beyond Lifshitz invariants. *Phys. Rev. B* **101**, 161403(R) (2020).

34. Perdew, J. P., Burke, K. & Ernzerhof, M. Generalized gradient approximation made simple. *Phys. Rev. Lett.* **77**, 3865 (1996).

35. Herring, C. Exchange Interactions Among Itinerant Electrons, in Magnetism, Vol. IV, (eds Rado, G. T. & Suhl, H. (Academic Press, 1966).

36. Sandratskii, L. M. Noncollinear magnetism in itinerant-electron systems: theory and applications. *Adv. Phys.* **47**, 91 (1998).

AUTHOR CONTRIBUTIONS
S.K., A.M.P., and T.O. designed the research, K.Y. fabricated the SLs, W.S.H. carried out the device fabrication, XRR and electrical measurements, W.S.H, K.K., S.K., and T.O. analyzed experimental data. A.M.P., S.R., and K.N. carried out and analyzed the DFT calculations. W.S.H., A.M.P., S.K., and T.O. wrote the manuscript with input from all the authors.

COMPETING INTERESTS
The authors declare no competing interests.

ADDITIONAL INFORMATION
Correspondence and requests for materials should be addressed to A.-M.P., S.K. or T.O.

Reprints and permission information is available at http://www.nature.com/reprints

Publisher's note Springer Nature remains neutral with regard to jurisdictional claims in published maps and institutional affiliations.